Exchange Controls Coarsening of Surface Condensates

Riccardo Rossetto,[1,2] Marcel Ernst,[1,2] and David Zwicker[1,*]
[1]Max Planck Institute for Dynamics and Self-Organization, Am Faßberg 17, 37077 Göttingen, Germany
[2]University of Göttingen, Institute for the Dynamics of Complex Systems, Friedrich-Hund-Platz 1, 37077 Göttingen, Germany

(Received 5 November 2025; accepted 13 April 2026; published 15 May 2026)

Biological membranes often exhibit heterogeneous protein patterns, which cells control. Strong patterns, like the polarity spot in budding yeast, can be described as surface condensates, formed by physical interactions between constituents. However, it is unclear how these interactions affect the material exchange with the bulk. To study this, we analyze a thermodynamically consistent model, which reveals that passive exchange generally accelerates the coarsening of surface condensates. Active exchange can further accelerate coarsening, although it can also fully arrest it and induce complex patterns involving various length scales. We reveal how these behaviors are related to nonlocal transport via diffusion through the bulk, rationalizing the various scaling laws that we observe and allowing us to interpret biologically relevant scenarios.

DOI: 10.1103/ndvb-yklf

Biological cells are enclosed by lipid membranes, which are crucial for interacting with the surroundings. These membranes are complex, and cells control their composition in space and time. In part, they achieve this by exploiting phase separation to form condensates embedded in the membrane [1–4]. One example is the polarity spot of budding yeast, which is a dense accumulation of multiple proteins at one region of the membrane, forming in preparation of cell division [5]. In this case, the proteins exchange with the bulk cytosol is apparently controlled by cells to ensure faithful division [6]. However, the general principles of controlling condensates in membranes by material exchange remain elusive.

Models of pattern formation on membranes have been discussed in various contexts ranging from cluster descriptions [7] to spatially resolved models. Prominent examples of the latter are reaction-diffusion models [8–12], which explain the emergence of patterns but cannot describe physical interactions required for phase separation. Phase separation has been included in various thermodynamic models, e.g., in the specific case of surface wetting [13–15] and in more general theories that prescribe fixed exchange rates [16,17]. However, it is unclear how thermodynamic constraints from physical interactions impact material exchange and the resulting patterns.

*Contact author: david.zwicker@ds.mpg.de

Published by the American Physical Society under the terms of the Creative Commons Attribution 4.0 International license. Further distribution of this work must maintain attribution to the author(s) and the published article's title, journal citation, and DOI. Open access publication funded by the Max Planck Society.

In this Letter, we develop a minimal, thermodynamically consistent model of phase separation in surfaces including passive and active material exchange with the bulk [Fig. 1(a)]. We find that passive exchange generally accelerates coarsening, whereas activity can either accelerate or suppress it, depending on details. We characterize the state of the surface by the area fraction field $\phi(\boldsymbol{r}, t)$ of solute molecules, so the solvent fraction is $1 - \phi(\boldsymbol{r}, t)$. By contrast, the state of the bulk is described by the mean solute fraction $\psi(t)$ since we assume fast diffusion in the bulk. The associated dynamics are governed by

$$\partial_t \phi(\boldsymbol{r}, t) = \Lambda \nabla^2 \mu_\mathrm{s}(\boldsymbol{r}, t) + s(\boldsymbol{r}, t) \tag{1a}$$

$$\partial_t \psi(t) = -\gamma \int_A s(\boldsymbol{r}, t) \mathrm{d}A, \tag{1b}$$

where Λ is the solute mobility on the surface. Equation (1b) describes the effect of the exchange flux s integrated over the entire surface A, and the parameter $\gamma = \nu_\mathrm{b}/(\nu_\mathrm{s} V)$ captures the relative size of the surface to the bulk with volume V. Here, ν_b denotes the molecular volume in the bulk, wheres ν_s is the molecular area in the surface. Finally, we express the exchange flux s as [18,19]

$$s = 2k_\mathrm{p} \sinh\left(\frac{\mu_\mathrm{b} - \mu_\mathrm{s}}{2k_\mathrm{B}T}\right) + 2k_\mathrm{a} \sinh\left(\frac{\mu_\mathrm{b} - \mu_\mathrm{s} - \Delta\mu}{2k_\mathrm{B}T}\right), \tag{2}$$

where $k_\mathrm{B}T$ sets the energy scale. The first term describes passive exchange proportional to the rate $k_\mathrm{p} > 0$. This exchange obeys detailed balance and is driven by the difference between the bulk chemical potential $\mu_\mathrm{b}(t)$ and the surface chemical potential $\mu_\mathrm{s}(\boldsymbol{r}, t)$, which quantify the increase in free energy when the solvent is replaced by a

solute particle in the bulk or surface, respectively. By contrast, the second term in Eq. (2) describes an active exchange proportional to the rate $k_a > 0$, where the chemical potential difference is biased by the external energy input $\Delta\mu$ provided by a fuel [18,20]. The two chemical potentials, $\mu_s = \nu_s \delta F[\phi,\psi]/\delta\phi$ and $\mu_b = (\nu_b/V)\partial F[\phi,\psi]/\partial\psi$, follow from the free energy F,

$$F[\phi,\psi] = \int_A \left[f_s(\phi) + \frac{\kappa}{2}|\nabla\phi|^2 \right] \mathrm{d}A + V f_b(\psi), \quad (3)$$

where the local free energy densities f_s and f_b govern the behaviors of homogeneous mixtures in the surface and bulk, respectively. Analyzing equilibrium states reveals that interesting behavior requires phase separation in the surface [21], which we describe by a Flory–Huggins energy, $f_s = k_B T \nu_s^{-1}[\chi\phi(1-\phi) + \phi\log(\phi) + (1-\phi)\times \log(1-\phi) + \omega_s\phi]$. Here, χ accounts for interactions driving phase separation, leading to the coexisting volume fractions $\phi_{in}^{(0)}$ and $\phi_{out}^{(0)}$ [22]. The gradient term proportional to κ in Eq. (3) penalizes concentration variations in the surface, leads to interfaces of finite width, and induces surface tension. We assume that interactions do not play a significant role in the bulk, which we thus describe as an ideal mixture, $f_b = k_B T/\nu_b[\psi\log(\psi) + \psi\omega_b]$. The energy difference $\omega_b - \omega_s$ controls the affinity of the molecules toward the surface, and we neglect explicit coupling terms describing wetting since they typically just lead to parameter rescaling [21]. Taken together, Eqs. (1)–(3) describe thermodynamically consistent dynamics of interacting solute molecules that can form patterns in the surface and exchange with the homogeneous bulk.

To understand the dynamics of phase separation in the surface, we first consider passive systems ($k_a = 0$). In particular, we perform numerical simulations of Eqs. (1)–(3) for a two dimensional surface with periodic boundary conditions [24], which leads to droplets of various sizes [Fig. 1(b)]. We quantify the dynamics of these droplets by their average radius as a function time [Fig. 1(c)]. Without exchange ($k_p = 0$, red line), Eq. (1a) reduces to regular Cahn–Hilliard dynamics [29], explaining the observed Lifshiz–Slyozov coarsening of $R \sim t^{1/3}$ [25,30]. Enabling passive exchange ($k_p > 0$, blue lines) accelerates coarsening, which is expected since the exchange provides an additional transport channel between droplets, akin to intermittent search strategies [31]. A linear stability analysis of the equations supports this conclusion since it shows that k_p increases the growth rate of perturbation modes with long wavelengths (Supplemental Material [23]). Beside the quantitative acceleration of the coarsening, we also observe a transition to a qualitatively different coarsening regime, where the coarsening law approaches $R \sim t^{1/2}$ for sufficiently large droplets. This observed scaling is reminiscent of the behavior of systems that do not conserve mass locally

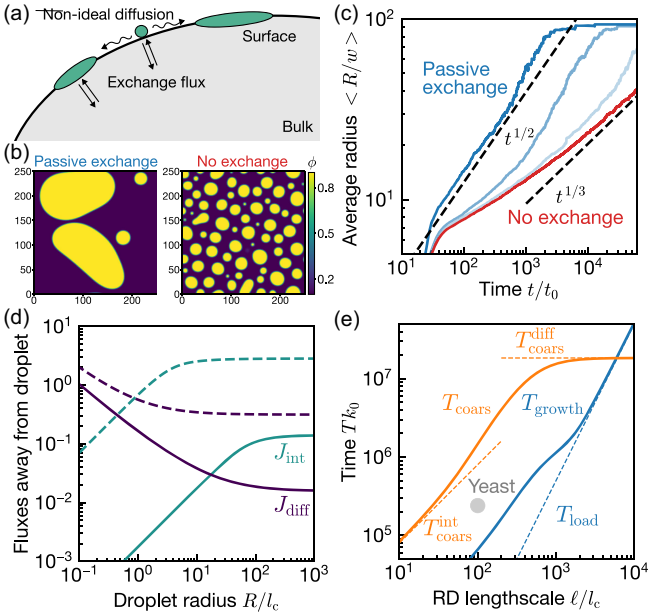


FIG. 1. Passive exchange with bulk accelerates coarsening in a surface. (a) Schematic of our model describing interacting solutes that phase separate in a 2D surface and exchanges with a 3D bulk. (b) Snapshots of the surface density ϕ from numerical simulations with and without passive exchange at the same time $t = 10^3 t_0$ for $\Phi_{tot} = 0.5$, $\chi = 3.5$, $\kappa = 2k_B T w^2/\nu_s$, $\omega_b - \omega_s = 6.5$, $\gamma A = 100$, $k_a = 0$, $w = (\nu_s\kappa/k_B T)^{1/2}$, and $t_0 = w^2/(k_B T\Lambda)$. (c) Mean droplet radius R as a function of t for $k_p = 0$ (red line) and $k_p t_0 = 10^{-3}, 10^{-2}, 10^{-1}$ (lighter to darker blue lines) for the same parameters as in (a). (d) Fluxes from a droplet toward the dilute phase (J_{diff}) and the bulk (J_{int}) as a function of radius R for reaction-diffusion lengths $\ell_{in} = \ell_{out} = \ell = 40 l_c$ (solid lines) and $\ell = 2l_c$ (dashed lines) for $\phi_{out}^{(0)} = 0.1$, $\phi_{in}^{(0)} = 0.9$, $k_0 = D/l_c^2$ with $D = D_{in} = D_{out}$. (e) Time scale of growing a single droplet (T_{growth}, blue line) and coarsening of two droplets (T_{coars}, orange line) as a function of ℓ compared to estimates for polarity spots in budding yeast (gray disk). Limiting cases T_{coars}^{diff}, T_{coars}^{int}, and T_{load} are discussed in the main text and Supplemental Material [23]. Parameters are $R_* = 10^2 l_c$, $L = 10^3 l_c$, $\Phi_{tot} = 0.5$, $\eta = 100$, $\phi_{dil} = 0.101$, and given in (d).

(model A dynamics or Allen–Cahn dynamics [32,33]), suggesting that the dynamics of large droplets are dominated by exchange while diffusion is negligible.

To study why passive exchange can alter coarsening qualitatively, we next evaluate the fluxes between droplets that formed in the surface. Focusing on an individual droplet of radius R, the equilibrium fractions $\phi_n^{eq} = \phi_n^{(0)}(1 + l_c/R)$ for $n \in \{\mathrm{in}, \mathrm{out}\}$ are slightly elevated by surface tension effects, which is quantified by the capillary length l_c [18]. We approximate the dynamics inside and outside the droplet by expanding Eq. (1) around the coexisting fractions $\phi_{in}^{(0)}$ and $\phi_{out}^{(0)}$,

$$\partial_t \phi_n \simeq D_n \nabla^2 \phi_n - k_n(\phi_n - \phi_n^{(0)}), \quad (4)$$

for $n \in \{\text{in}, \text{out}\}$ (Supplemental Material [23]). Combining the diffusivities $D_n \simeq \Lambda \nu_s f_s''(\phi_n^{(0)})$ and rate constants $k_n = -s'(\phi_n^{(0)})$, we define reaction-diffusion length scales $\ell_n = (D_n/k_n)^{1/2}$, which quantify how far solute molecules diffuse in the surface before unbinding. Mass balance implies the droplet growth rate [18]

$$\frac{\mathrm{d}R}{\mathrm{d}t} = -\frac{J_{\text{diff}} + J_{\text{int}}}{2\pi R(\phi_{\text{in}}^{(0)} - \phi_{\text{out}}^{(0)})}, \tag{5}$$

where $J_{\text{diff}} = -2\pi R D_{\text{out}} \phi_{\text{out}}'(R)$ denotes the diffusive flux from the interface to the surrounding dilute phase, whereas J_{int} captures the internal unbinding flux from the droplet to the bulk, $J_{\text{int}} = 2\pi k_{\text{in}} \int_0^R r[\phi_{\text{in}}(r) - \phi_{\text{in}}^{(0)}]\mathrm{d}r$ for a polar symmetric system in the quasistationary limit. Both fluxes can be determined analytically [Appendix A and Fig. 1(d)], revealing their influence on the dynamics. For fast exchange ($R \gg \ell_n$) both fluxes are interface limited, implying an $R \sim t^{1/2}$ scaling. In the opposite limit of slow exchange ($R \ll \ell_n$), J_{diff} dominates and leads to the expected $R \sim t^{1/3}$ scaling. These results are consistent with our numerical simulations [Fig. 1(c)].

We next use the effective fluxes to predict timescales of polarity spot formation in budding yeast. Detailed analysis in Appendix B and Fig. 1(e) reveal that spot formation is limited by the exchange rate (for large ℓ) or by transport within the surface (for small ℓ). The associated time T_{growth} is faster than polarity spot formation in yeast, implying that passive exchange could explain it. However, budding yeast occasionally exhibits multiple polarity spots, which need to be resolved by coarsening. For passive exchange, our analysis reveals that the associated coarsening time scale T_{coars} is too large to match experiments [Fig. 1(e)], suggesting that experimentally observed activity [5] could be crucial to forming polarity spots quickly and robustly.

To study active unbinding from the surface ($k_a \neq 0$), we first consider the simple case where the exchange is independent of position ($k_p, k_a, \Delta\mu$ constant), in which the behavior is qualitatively similar to the passive case. To see this, we linearize the exchange flux given by Eq. (2) using $\sinh(x) \approx x$, which implies $s_p = -s_a \approx \Delta\mu k_p k_a/[k_B T(k_p + k_a)]$ at stationarity. The system thus never reaches equilibrium when k_a and $\Delta\mu$ are finite. Specifically, for $\Delta\mu > 0$, material is removed from the surface using the external energy input, whereas it rebinds through the passive exchange flux. However, if the rates k_p and k_a are constants, these fluxes are balanced everywhere, leading to futile cycles, which do not alter the dynamics [20].

To find interesting behavior, we need to break the futile cycles so that binding toward the surface at one place is balanced by unbinding at another place. To do this, we consider constant k_p combined with composition-dependent active unbinding,

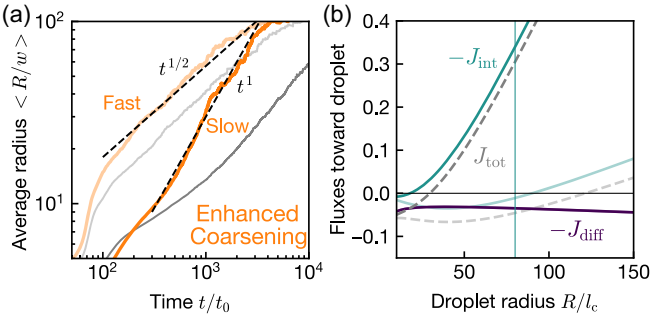


FIG. 2. Active unbinding from dilute regions accelerates coarsening. (a) Mean droplet radius R as a function of time t for $\alpha = -0.5$ (active system, orange line) and $\alpha = 0$ (passive system, gray line) as well as $k = 10^{-1}/t_0$ (light colors) and $k = 10^{-2}/t_0$ (dark colors). Parameters are $\Delta\mu = 2k_B T$ and given in Figs. 1(b) and 1(c). (b) Diffusive efflux J_{diff} and internal unbinding flux J_{int} as a function of R for $\Delta\phi_{\text{in}} = 0.01$ (light colors) and $\Delta\phi_{\text{in}} = 0.05$ (dark colors). Gray dashed line corresponds to $J_{\text{tot}} = J_{\text{diff}} + J_{\text{int}}$. Vertical line indicates estimated transition between area- and interface-limited flux J_{int} (Supplemental Material [23]). Model parameters are $\Delta\phi_{\text{out}} = -10^{-3}$, $\ell = 40 l_c$, and given in Figs. 1(d) and 1(e).

$$k_p = k \quad k_a = k\left[\frac{1+\alpha}{2}\phi + \frac{1-\alpha}{2}(1-\phi)\right], \tag{6}$$

motivated by enzymes segregating into droplets [20]. For simplicity, we here assume that passive and active exchanges occur with similar rate k, but the active flux is modified by the asymmetry parameter $\alpha \in [-1, 1]$. For $\alpha > 0$ and $\Delta\mu > 0$, active unbinding happens predominately inside droplets, where ϕ is large. Conversely, for $\alpha < 0$ (but still $\Delta\mu > 0$), the active flux is biased toward dilute regions, and $\alpha = 0$ corresponds to homogeneous active exchange, which exhibits passive dynamics. We can thus use α to control the direction of circular fluxes between dense and dilute surface regions and the bulk.

We first focus on the case where activity promotes unbinding from dilute regions ($\alpha < 0$). Figure 2(a) shows that such activity (orange lines) accelerates coarsening compared to the passive case (gray lines). The data suggests that not only is the prefactor increased but also the coarsening exhibits a different power law, where the average droplet radius scales linearly with time for slower exchange. To understand this behavior, we again study the fluxes J_{diff} and J_{int} affecting a droplet of radius R. In contrast to the passive case discussed above, the exchange flux now does not vanish at phase equilibrium [$\phi_{\text{in}} = \phi_{\text{in}}^{(0)}$ and $\phi_{\text{out}} = \phi_{\text{out}}^{(0)}$]. The difference between phase equilibrium and exchange equilibrium is quantified by fractions $\Delta\phi_n$, which imply the following reaction-diffusion equations in the phases $n = \text{in}, \text{out}$ [19,34]:

$$\partial_t \phi_n \simeq D_n \nabla^2 \phi_n - k_n(\phi_n - \phi_n^{(0)} - \Delta\phi_n), \tag{7}$$

where $k_n = -s'(\phi_n^{(0)})$ and $\Delta\phi_n = s(\phi_n^{(0)})/k_n$. For passive systems ($\Delta\phi_n = 0$), this equation is identical to Eq. (4). Consequently, the associated fluxes J_{diff} and J_{int} can be obtained via replacing $\phi_n^{(0)}$ by $\phi_n^{(0)} + \Delta\phi_n$ in Eqs. (A1) and (A2), respectively. For $\alpha < 0$, we find $\Delta\phi_{\mathrm{out}} < 0$ and $\Delta\phi_{\mathrm{in}} > 0$, which enables systems where J_{int} dominates for small droplets [$R \ll \ell_{\mathrm{in}}$, Fig. 2(b), which is impossible in passive systems, Fig. 1(d), for $\ell_{\mathrm{in}} = \ell_{\mathrm{out}}$]. In this case, we predict ballistic growth ($R \sim t$), consistent with our data [Fig. 2(a)], and even superlinear scalings become accessible for strong activity (Supplemental Material [23]). However, our theory predicts a transition to $R \sim t^{1/2}$ when droplets are sufficiently large, so J_{int} eventually becomes interface limited. For faster exchange rates, this transition takes place at smaller droplets, implying that $R \sim t^{1/2}$ is observed earlier, consistent with data [Fig. 2(a)].

Overall, our numerical simulations indicate that active unbinding in dilute regions accelerates coarsening. Qualitatively, this is because active unbinding effectively undersaturates the dilute region ($\Delta\phi_{\mathrm{out}} < 0$), while adding material to dense regions ($\Delta\phi_{\mathrm{in}} > 0$). The resulting circular fluxes enhance material transport from small to large droplets, thus accelerating coarsening. To investigate this acceleration quantitatively, we again estimate the time T_{coars} needed to resolve two spots separated by L. Using the same technique as above and considering parameters compatible with polarity formation in budding yeast, we find that a relatively small energy input ($\Delta\mu = 2k_{\mathrm{B}}T$) can lead to significant acceleration ($T_{\mathrm{coars}}^{\mathrm{act}} \sim 10^2$ s, Supplemental Material [23]). This suggests that budding yeast uses active processes to promote unbinding from dilute regions to ensure the formation of a single polarity spot quickly and robustly.

In the opposing case where activity promotes unbinding from dense regions ($\alpha > 0$), coarsening is slowed [Fig. 3(a)]. Interestingly, the slowdown is strongest for intermediate exchange rates (pink line), where it seems to halt completely. To understand this slowdown, we again study the total flux toward the droplet, $J_{\mathrm{tot}} = -J_{\mathrm{int}} - J_{\mathrm{diff}}$, which governs droplet growth; see Eq. (5). For $\alpha > 0$, we find $\Delta\phi_{\mathrm{out}} > 0$ and $\Delta\phi_{\mathrm{in}} < 0$, Supplemental Material [23], which implies that J_{tot} exhibits two roots [Fig. 3(b)]. While the first root corresponds to the critical radius below which droplets shrink, the second root is a stable state, indicating that droplets of that size are stable. This situation is akin to externally maintained droplets where chemical conversion of material drives similar fluxes, leading to arrested coarsening [18,20,34]. This similarity is also supported by linear stability analysis (Supplemental Material [23]), which reveals a band of unstable modes. Taken together, material exchange between surface and bulk plays a similar role to the previously described reactions in bulk. Intuitively, the arrested coarsening is caused by active unbinding from the dense region ($\Delta\phi_{\mathrm{in}} < 0$) and rebinding at the dilute region ($\Delta\phi_{\mathrm{out}} > 0$). The resulting fluxes

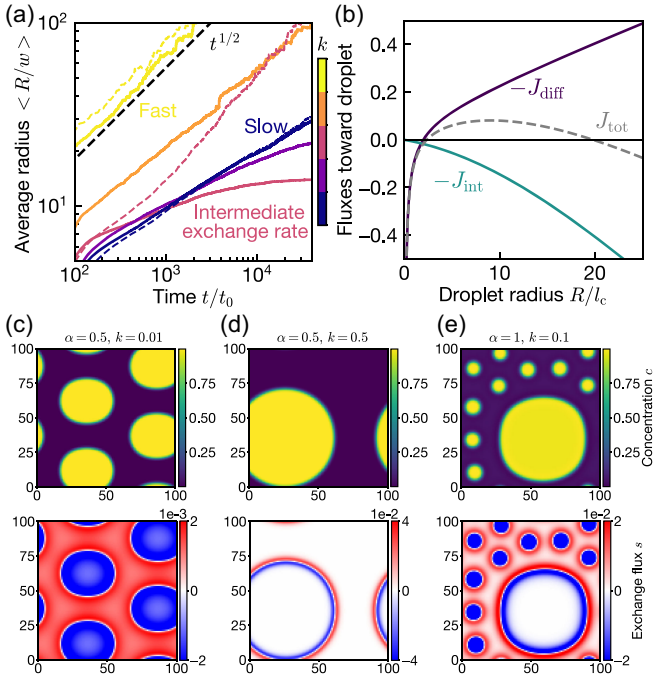


FIG. 3. Active unbinding from dense regions can arrest coarsening. (a) Mean droplet radius R as a function of time t for $\alpha = 0.5$, $\Delta\mu = 2k_{\mathrm{B}}T$, and $kt_0 = 5 \times 10^{-1}, 10^{-1}, 10^{-2}, 10^{-3}, 10^{-4}$ (fast to slow). Dashed curves corresponds to passive limits ($\alpha = 0$). Remaining parameters are given in Figs. 1(b) and 1(c). (b) Diffusive efflux and internal unbinding fluxes for $\Delta\phi_{\mathrm{in}} = -0.1$, $\Delta\phi_{\mathrm{out}} = 0.05$, $\ell = 10l_{\mathrm{c}}$. Remaining parameters and units are given in Figs. 1(d) and 1(e). The gray dashed line corresponds to $J_{\mathrm{tot}} = J_{\mathrm{diff}} + J_{\mathrm{int}}$. (c)–(e) Stationary concentration field $c(\boldsymbol{r}, t)$ (top panels) and corresponding exchange fluxes (bottom panels) for various parameters: (c) $k = 10^{-2}/t_0$ [corresponding to pink line in panel (a)], (d) $k = 5 \times 10^{-1}/t_0$ [yellow line in panel (a)], and (e) $\alpha = 1$ with $\chi = 3$, $\Phi_{\mathrm{tot}} = 0.6$, and $k = 0.1$. Remaining parameters are the same as in panel (a).

transport material from large to small droplets, thus opposing coarsening and supporting regular hexagonal patterns [Fig. 3(c)]. From analyzing chemically active droplets, we expect that smaller reaction rates (i.e., exchange rates in our case) lead to patterns with larger length scale [35–39]. Figure 3(a) indeed suggests that slower exchange affects coarsening less (blue line), and we predict that the average droplet radius reaches a stable stationary state eventually. Taken together, we find that size control of droplets eventually limits coarsening.

We have shown that larger exchange rates arrest droplets at smaller sizes, implying a stronger suppression of coarsening. While this is confirmed by Fig. 3(a), very large exchange rates surprisingly lead to fast coarsening again, which hardly differs from the passive case [yellow line in Fig. 3(a)]. In these cases, we do not observe any size control, and the system instead coarsens toward a single droplet [Fig. 3(d)]. The droplet sizes evolve as $R(t) \sim t^{1/2}$, consistent with passive exchange [Fig. 1(c)]. For the large

rates considered here, the exchange becomes interface limited [Fig. 3(d)], implying a correction to the interface behavior, whereas phase coexistence behaves effectively as a passive system [40,41]. Taken together, this suggest that strong reactions merely affect the interface, but the large-scale behavior is essentially unchanged.

In the case where activity promotes unbinding from dense regions, faster exchange kinetics (large k) generally accelerate coarsening when size control is not yet relevant [early times in Fig. 3(a)], similar to passive exchange. However, in some cases active unbinding from dense regions introduces fluxes between droplets that can limit their sizes. This size control sets in earlier for larger exchange rates k [39], explaining the observed earlier slowdown of coarsening [e.g., pink curve in Fig. 3(a)]. However, for even larger k, we do not observe any size control, and instead the system coarsens indefinitely. This distinction between size control and coarsening suggests that there is a critical exchange rate, although we also observe multistability, where the behavior depends on initial conditions (Fig. S2 in Supplemental Material [23]). Interestingly, we sometimes even observe coexistence between multiple droplets of equal size and a single large droplet [Fig. 3(e)], which we interpret as coexistence between a patterned phase and a dense macrophase. In that case, we observe continuous coarsening of the macrophase, whereas the patterned phase plays the role of the dilute phase.

In summary, we showed that passive exchange accelerates coarsening (Fig. 1), whereas active exchange either accelerates (Fig. 2) or suppresses coarsening (Fig. 3). The precise coarsening dynamics depend on how droplets exchange material, which either happens by diffusion along the surface or via diffusion through the bulk upon unbinding. The exchange dynamics determine whether these fluxes are limited to regions around the interface or not, which affects the coarsening dynamics qualitatively. The suppressed coarsening is akin to chemically active droplets [18,19,34], which also exhibit multistability [39,42]. Beyond these similarities, we additionally observe the coexistence of many small droplets with one large homogeneous region [Fig. 3(e)]. Interestingly, similar patterns have been observed in phase-field crystals [43], systems with nonlocal elasticity [44], and chemically active ternary mixtures [45]. We hypothesized in a recent manuscript that all of these examples can be effectively described as equilibrium states of systems that combine phase coexistence with nonlocal interactions [46]. The exchange dynamics of the present work should correspond to long-range interactions since they are akin to chemical conversions [35–38,46]. Such long-range interactions introduce an extra constraint ensuring that the free energy is extensive [37,47,48], such as charge neutrality for electrostatic interactions. This additional constraint prohibits phase coexistence in binary mixtures according to the Gibbs phase rule [49]. However, in our system, the bulk compartment can be interpreted as an additional component, which adds a degree of freedom, thus allowing two coexisting phases [21]. Taken together, this suggests the possible stationary states in our system are constrained by the Gibbs phase rule, which permits up to two coexisting phases, of which one can be patterned due to the long-range interactions induced by the exchange.

Our results have implications for membrane patterns in biology. For instance, we propose that active exchange is necessary to quickly and robustly form only one polarity spot in budding yeast. However, our general theory applies to many pattern forming systems, including PAR protein patterns in *C. elegans* [50], postsynaptic densities in neurons [51], protein clusters in bacterial membranes [52], Min protein patterns [12,53,54], and Noc proteins *in vitro* [55]. To describe these systems in detail, our model likely needs to be extended, e.g., by including dimerization [21,56], advection [57], exchange with linear compartments [58,59], chemical reactions, membrane interactions [60,61], and fluctuations [62].

Acknowledgments—We thank Nynke Hettema, Kueyoung Kim, Stefan Köstler, Guido Kusters, Liedewij Laan, Filipe Thewes, and Gerrit Wellecke for helpful discussions. We gratefully acknowledge funding from the Max Planck Society and the European Union (ERC, EmulSim, No. 101044662).

Data availability—The data that support the findings of this article are openly available [63].

[1] S. Banjade and M. K. Rosen, eLife **3**, e04123 (2014).
[2] D. B. McAffee, M. K. O'Dair, J. J. Lin, S. T. Low-Nam, K. B. Wilhelm, S. Kim, S. Morita, and J. T. Groves, Nat. Commun. **13**, 7446 (2022).
[3] T. Litschel, C. F. Kelley, X. Cheng, L. Babl, N. Mizuno, L. B. Case, and P. Schwille, Nat. Commun. **15**, 4986 (2024).
[4] A. Kamatar, J. P. K. Bravo, F. Yuan, L. Wang, E. M. Lafer, D. W. Taylor, J. C. Stachowiak, and S. H. Parekh, Biophys. J. **123**, 1494 (2024).
[5] J.-g. Chiou, M. K. Balasubramanian, and D. J. Lew, Annu. Rev. Cell Dev. Biol. **33**, 77 (2017).
[6] M.-P. Gulli, M. Jaquenoud, Y. Shimada, G. Niederhäuser, P. Wiget, and M. Peter, Mol. Cell **6**, 1155 (2000).
[7] M. S. Turner, P. Sens, and N. D. Socci, Phys. Rev. Lett. **95**, 168301 (2005).
[8] C. F. Lang and E. M. Munro, Biophys. J. **121**, 4543 (2022).
[9] K. John and M. Bär, Phys. Rev. Lett. **95**, 198101 (2005).
[10] K. John and M. Bär, Phys. Biol. **2**, 123 (2005).
[11] R. Geßele, J. Halatek, L. Würthner, and E. Frey, Nat. Commun. **11**, 539 (2020).
[12] F. Brauns, G. Pawlik, J. Halatek, J. Kerssemakers, E. Frey, and C. Dekker, Nat. Commun. **12**, 3312 (2021).
[13] X. Zhao, G. Bartolucci, A. Honigmann, F. Jülicher, and C. A. Weber, New J. Phys. **23**, 123003 (2021).
[14] X. Zhao, S. Liese, A. Honigmann, F. Jülicher, and C. A. Weber, New J. Phys. **26**, 103025 (2024).

[15] X. Zhao, D. Sun, G. Bartolucci, A. A. Hyman, A. Honigmann, and C. A. Weber, eLife (2025).
[16] L. Foret, Europhys. Lett. **71**, 508 (2005).
[17] N. Caballero, K. Kruse, and T. Giamarchi, Phys. Rev. E **108**, L012801 (2023).
[18] D. Zwicker, O. Paulin, and C. ter Burg, Rep. Prog. Phys. **88**, 116601 (2025).
[19] D. Zwicker, Curr. Opin. Colloid Interface Sci. **61**, 101606 (2022).
[20] J. Kirschbaum and D. Zwicker, J. R. Soc. Interface **18**, 20210255 (2021).
[21] R. Rossetto, G. Wellecke, and D. Zwicker, Phys. Rev. Res. **7**, 023145 (2025).
[22] D. Qian, T. C. T. Michaels, and T. P. J. Knowles, J. Phys. Chem. Lett. **13**, 7853 (2022).
[23] See Supplementl Material at http://link.aps.org/supplemental/10.1103/ndvb-yklf for the derivation of Eq. (4), linear stability analysis, details on the scaling behavior of the internal and diffusive fluxes and on the estimation of timescales, and evidence for multistability related to Fig. 3(a), which includes Refs. [18,21,24–28].
[24] D. Zwicker, J. Open Source Software **5**, 2158 (2020).
[25] I. Lifshitz and V. Slyozov, J. Phys. Chem. Solids **19**, 35 (1961).
[26] A. Kulkarni, E. Vidal-Henriquez, and D. Zwicker, Sci. Rep. **13**, 733 (2023).
[27] C. Wagner, Z. Elektrochem. Ber. Bunsenges. Phys. Chem. **65**, 581 (1961).
[28] C. F. Lee, Phys. Rev. Res. **3**, 043081 (2021).
[29] J. W. Cahn and J. E. Hilliard, J. Chem. Phys. **28**, 258 (1958).
[30] J. A. Marqusee, J. Chem. Phys. **81**, 976 (1984).
[31] O. Bénichou, C. Loverdo, M. Moreau, and R. Voituriez, Rev. Mod. Phys. **83**, 81 (2011).
[32] J. Rubinstein and P. Sternberg, IMA J. Appl. Math. **48**, 249 (1992).
[33] A. Bray, Adv. Phys. **43**, 357 (1994).
[34] C. A. Weber, D. Zwicker, F. Jülicher, and C. F. Lee, Rep. Prog. Phys. **82**, 064601 (2019).
[35] S. C. Glotzer and A. Coniglio, Phys. Rev. E **50**, 4241 (1994).
[36] J. J. Christensen, K. Elder, and H. C. Fogedby, Phys. Rev. E **54**, R2212 (1996).
[37] C. B. Muratov, Phys. Rev. E **66**, 066108 (2002).
[38] D. Zwicker, A. A. Hyman, and F. Jülicher, Phys. Rev. E **92**, 012317 (2015).
[39] S. Köstler, Y. Qiang, G. Kusters, and D. Zwicker, Phys. Rev. Res. **8**, 013107 (2026).
[40] Y. Qiang, C. Luo, and D. Zwicker, Phys. Rev. Lett. **135**, 268301 (2025).
[41] Y. Cho and W. M. Jacobs, Proc. Natl. Acad. Sci. U.S.A. **122**, e2501145122 (2025).
[42] J. Bauermann, G. Bartolucci, J. Boekhoven, F. Jülicher, and C. A. Weber, Phys. Rev. X **15**, 041027 (2025).
[43] U. Thiele, A. J. Archer, M. J. Robbins, H. Gomez, and E. Knobloch, Phys. Rev. E **87**, 042915 (2013).
[44] Y. Qiang, C. Luo, and D. Zwicker, Phys. Rev. X **14**, 021009 (2024).
[45] G. Bartolucci, O. Adame-Arana, X. Zhao, and C. A. Weber, Biophys. J. **120**, 4682 (2021).
[46] F. C. Thewes, Y. Qiang, O. W. Paulin, and D. Zwicker, arXiv:2511.05214.
[47] T. Ohta and K. Kawasaki, Macromolecules **19**, 2621 (1986).
[48] F. Liu and N. Goldenfeld, Phys. Rev. A **39**, 4805 (1989).
[49] J. W. Gibbs, Trans. Conn. Acad. Arts Sci. **3**, 1 (1876).
[50] C. F. Lang and E. Munro, Development **144**, 3405 (2017).
[51] M. Zeng, Y. Shang, Y. Araki, T. Guo, R. L. Huganir, and M. Zhang, Cell **166**, 1163 (2016).
[52] G. Benn, I. V. Mikheyeva, P. G. Inns, J. C. Forster, N. Ojkic, C. Bortolini, M. G. Ryadnov, C. Kleanthous, T. J. Silhavy, and B. W. Hoogenboom, Proc. Natl. Acad. Sci. U.S.A. **118**, e2112237118 (2021).
[53] M. Loose, K. Kruse, and P. Schwille, Annu. Rev. Biophys. **40**, 315 (2011).
[54] L. Würthner, F. Brauns, G. Pawlik, J. Halatek, J. Kerssemakers, C. Dekker, and E. Frey, Proc. Natl. Acad. Sci. U.S.A. **119**, e2206888119 (2022).
[55] L. Babl, A. Merino-Salomón, N. Kanwa, and P. Schwille, Sci. Rep. **12**, 17949 (2022).
[56] T. Bland, N. Hirani, D. C. Briggs, R. Rossetto, K. Ng, I. A. Taylor, N. Q. McDonald, D. Zwicker, and N. W. Goehring, EMBO J. **43**, 3214 (2024).
[57] N. W. Goehring, P. K. Trong, J. S. Bois, D. Chowdhury, E. M. Nicola, A. A. Hyman, and S. W. Grill, Science **334**, 1137 (2011).
[58] M. Ernst, R. Rossetto, and D. Zwicker, PRX Life **4**, 013033 (2026).
[59] J. A. Morin, S. Wittmann, S. Choubey, A. Klosin, S. Golfier, A. A. Hyman, F. Jülicher, and S. W. Grill, Nat. Phys. **18**, 271 (2022).
[60] Q. Yu and A. Košmrlj, Soft Matter **21**, 4288 (2025).
[61] A. Winter, Y. Liu, A. Ziepke, G. Dadunashvili, and E. Frey, Phys. Rev. E **111**, 044405 (2025).
[62] N. Ziethen, J. Kirschbaum, and D. Zwicker, Phys. Rev. Lett. **130**, 248201 (2023).
[63] R. Rossetto, M. Ernst, and D. Zwicker, Python code for the article "Exchange controls coarsening of surface condensates," Zenodo (2026), 10.5281/zenodo.19610241.
[64] D. M. Rutkowski, V. Vincenzetti, D. Vavylonis, and S. G. Martin, Nat. Commun. **15**, 8363 (2024).

End Matter

Appendix A: Effective fluxes—To obtain an expression for the flux J_{diff} from the droplet interface toward the dilute phase, we solve Eq. (4) at stationarity assuming polar symmetry. Using the boundary condition $\phi_{\mathrm{out}}(R) = \phi^{\mathrm{eq}}_{\mathrm{out}}(R)$ at the interface and no-flux conditions far away from the droplet, we find

$$J_{\mathrm{diff}} = 2\pi R \frac{D_{\mathrm{out}}}{\ell_{\mathrm{out}}} \frac{K_1(R/\ell_{\mathrm{out}})}{K_0(R/\ell_{\mathrm{out}})} \left(\phi^{\mathrm{eq}}_{\mathrm{out}}(R) - \phi^{(0)}_{\mathrm{out}}\right), \quad \text{(A1)}$$

where K_0, K_1 are modified Bessel functions of the second kind. If the exchange is slow ($R \ll \ell_{\mathrm{out}}$), J_{diff} behaves as a purely diffusive flux and J_{int} is negligible, leading to the expected Lifshitz–Slyozov scaling of $R \sim t^{1/3}$. In the converse limit ($R \gg \ell_{\mathrm{out}}$), fast exchange implies a homogeneous dilute phase, $\phi_{\mathrm{out}}(r) = \phi_{\mathrm{out}}^{(0)}$, so J_{diff} becomes proportional to the size of the droplet's interface, implying $R \sim t^{1/2}$ [27,28] (Supplemental Material [23]).

The internal unbinding flux J_{int} follows from an analogous evaluation of the profile $\phi_{\mathrm{in}}(r)$ with boundary conditions $\phi_{\mathrm{in}}(R) = \phi_{\mathrm{in}}^{\mathrm{eq}}(R)$ and $\phi_{\mathrm{in}}'(r=0) = 0$,

$$J_{\mathrm{int}} = 2\pi R \frac{D_{\mathrm{in}}}{\ell_{\mathrm{in}}} \frac{I_1(R/\ell_{\mathrm{in}})}{I_0(R/\ell_{\mathrm{in}})} \left(\phi_{\mathrm{in}}^{\mathrm{eq}}(R) - \phi_{\mathrm{in}}^{(0)}\right), \quad \text{(A2)}$$

where I_0, I_1 are modified Bessel functions of the first kind. For slow exchange ($R \ll \ell_{\mathrm{in}}$), diffusion equilibrates the profile inside the droplet, $\phi_{\mathrm{in}}(r) \simeq \phi_{\mathrm{in}}^{\mathrm{eq}}(R)$, so J_{int} becomes proportional to the droplet's area. Assuming that internal unbinding dominates transport ($J_{\mathrm{diff}} \simeq 0$), this regimes leads to a linear scaling $R \sim t$. Conversely, if $R \gg \ell_{\mathrm{in}}$, the material unbinds before being able to diffuse across the droplet, so material exchange is confined to a region close to the interface, implying $R \sim t^{1/2}$. These coarsening laws are indeed observed in effective numerical simulations (Supplemental Material [23]).

The effective fluxes allow us to interpret the numerically observed coarsening [Fig. 1(c)]. When the exchange is fast in both phases ($R \gg \ell_n$), the internal unbinding flux J_{int} behaves as an interface flux and dominates transport [Fig. 1(d)], leading to the scaling $R \sim t^{1/2}$ observed for the dark blue curve in Fig. 1(c). Conversely, when the exchange is slow ($R \ll \ell_n$), diffusion dominates [$J_{\mathrm{diff}} \gg J_{\mathrm{int}}$, Fig. 1(d)], implying $R \sim t^{1/3}$. For intermediate exchange kinetics [light blue curves in Fig. 1(c)], we find that diffusion dominates early, when droplets are small and close to each other, whereas exchange dominates later for large droplets that are far apart. By contrast, the ballistic regime ($R \sim t$), is inaccessible because it would require large J_{int} in the slow exchange regime ($R \ll \ell_n$) where J_{diff} dominates instead; see Fig. 1(d). Our analysis highlights that the two different fluxes can lead to qualitatively different coarsening regimes, which further depend on the relative size of droplets to the reaction-diffusion length scale.

Appendix B: Time scale estimation—We use the effective fluxes to approximate the relevant timescales governing the dynamics of single droplets and droplet pairs, where we for simplicity consider $\ell_{\mathrm{in}} = \ell_{\mathrm{out}} = \ell$ and $D_{\mathrm{in}} = D_{\mathrm{out}} = D$. We start by estimating how long it takes to form one large, stationary droplet in a finite system [38]. We estimate the corresponding time scale T_{growth} from a linear stability analysis around this stationary state in the Supplemental Material [23]. This time scale describes the exchange of material between bulk and surface, which is slow for large ℓ [Fig. 1(e)]. In this limit, T_{growth} is simply given by $T_{\mathrm{load}} \sim \ell^2/2D$, which describes homogeneous exchange. By contrast, for small ℓ, a droplet in the surface exchanges material with the bulk only in a region close to its interface. Our analysis shows that T_{growth} grows with ℓ, highlighting that passive exchange accelerates droplet formation. For a passive system, multiple droplets always coarsen until one droplet remains. We estimate the corresponding coarsening time T_{coars} from the rate at which the sizes of droplets separated by a distance L diverge. Figure 1(e) shows that T_{coars} exceeds T_{growth}, essentially because material exchange between droplets is slower than exchange with the bulk. Moreover, the two time scales exhibit different scaling laws as a function of ℓ. For fast exchange ($R, L \gg \ell$), we find (Supplemental Material [23])

$$T_{\mathrm{coars}}^{\mathrm{int}} \simeq \frac{R_*^2 \ell (\phi_{\mathrm{in}}^{(0)} - \phi_{\mathrm{out}}^{(0)})}{D l_c (\phi_{\mathrm{out}}^{(0)} + \phi_{\mathrm{in}}^{(0)})}, \quad \text{(B1)}$$

which is independent of the separation L since diffusive and internal unbinding fluxes are interface limited. By contrast, for slow exchange ($R, L \ll \ell$), the internal unbinding flux is area limited and molecules diffusing between droplets rarely unbind from the surface, leading to the timescale

$$T_{\mathrm{coars}}^{\mathrm{diff}} \simeq \frac{R_*^3 \log(L/R_*)(\phi_{\mathrm{in}}^{(0)} - \phi_{\mathrm{out}}^{(0)})}{D l_c \phi_{\mathrm{out}}^{(0)}}, \quad \text{(B2)}$$

which is independent of ℓ because the dynamics are essentially confined to the surface.

We next compare the estimated time scales to experimental measurements of polarity spots in budding yeast [5]. We estimate the diffusivity $D \sim 0.2\ \mu\mathrm{m}^2/\mathrm{s}$ and the exchange rate $k \sim 0.2\ \mathrm{s}^{-1}$ using measured values for the key protein Cdc42 [64]. Additionally assuming a capillary length of $l_c \sim 10$ nm based on molecular sizes and considering two polarity spots of size $R_* \sim 1\ \mu$m at distance $L \sim 10\ \mu$m, we find $T_{\mathrm{growth}} \sim 30$ s and $T_{\mathrm{coars}} \sim 7 \times 10^2$ s. Since polarity spots form within about two minutes, this suggests that passive exchange is consistent with their formation, but it fails to account for sufficiently fast resolution of two spots. Instead, we would expect that evolution devised a process that resolves multiple spots significantly more quickly to ensure robust formation of the polarity spot. This suggests that the experimentally observed activity [5] is crucial.